Available online at www.sciencedirect.com

jmr&t Journal of Materials Research and Technology

www.jmrt.com.br

Original Article

Magnetic filter produced by $ZnFe_2O_4$ nanoparticles using freeze casting☆

Letícia dos Santos Aguilera[a,*], *Rubens Lincoln Santana Blazutti Marçal*[a], *José Brant de Campos*[b], *Marcelo Henrique Prado da Silva*[a], *André Ben-Hur da Silva Figueiredo*[a]

[a] *Military Institute of Engineering – IME, Mechanical and Materials Engineering Department, Sq General Tibúrcio, 80, Praia Vermelha, Rio de Janeiro, RJ, Brazil*

[b] *State University of Rio de Janeiro – UERJ, Mechanical Engineering Department, São Francisco Xavier St, 524, Maracanã, Rio de Janeiro, RJ, Brazil*

ARTICLE INFO

Article history:
Received 20 November 2017
Accepted 24 April 2018
Available online 22 June 2018

Keywords:
Magnetic nanoparticles
Freeze casting
Zinc ferrite nanoparticles
Magnetic filters

ABSTRACT

Zinc ferrite magnetic nanoparticles were synthesized by combustion method and the obtained powders were processed by the freeze casting technique, to produce magnetic filters. Green bodies were obtained by freezing a water-based slurry of nanoparticles and polyethylene glycol (PEG) of molecular mass 8000. The suspension was frozen to −140 °C under the cooling rate of 10 °C/min. The obtained bodies were sintered at 1300 °C during 1 h and the X-ray diffraction (XRD) analyses showed ferrite as the only crystalline phase. Scanning electron microscopy (SEM) analyses revealed formation of porous channels in freezing direction and Archimedes' density measurements showed porosity values ranging from 48.0% to 63.0%, depending on PEG content.

1. Introduction

The various technological applications involving magnetic ferrite nanoparticles have been gaining prominence [1–7], with ongoing studies on the chemical, electrical, photoelectric, thermal and magnetic properties of these nanoparticles [8–15]. There are several syntheses routes, such as sol-gel, high energy milling and co-precipitation [12,16–19]. Among the most common methods, solution combustion synthesis is the simplest, quickest and most economical, thus producing high purity nanostructured ceramic powders without the use of further thermal treatments [20,21].

Composite materials based on polymeric, ceramic or metallic matrices reinforced with ferrite nanoparticles have been reported as biomedical materials, drug delivery systems, magnetic contrast agents, catalysts, pigments, purifiers and

☆ Paper was part of technical contributions presented in the events part of the ABM Week 2017, October 2nd to 6th, 2017, São Paulo, SP, Brazil.

* *Corresponding author.*
E-mail: le_aguilera13@hotmail.com (L.S. Aguilera).

https://doi.org/10.1016/j.jmrt.2018.04.012

removing agents such as ions, impurities and microorganisms present on water [22–26].

Freeze casting technique consists of fabricating porous ceramic bodies from a ceramic slurry, that is frozen. The solvent is removed by sublimation and the obtained green body is sintered [27,28]. Factors such as concentration of solids in the slurry, cooling rate and additives such as binders, influence the developed microstructure [29,30].

It is a promising technique for the production of bioceramics, since the porous struts are compatible with porous spongy bone. However, the strut may also be used in applications such as catalysis, where large surface area and the presence of macro, meso and micropores are required [27,29]. Another positive point is the fact that the manufacturing process is a sustainable route, since it is applicable to a wide variety of ceramics such as silicon carbide, silicon nitride, alumina, copper oxide, iron oxide, hydroxyapatite, titanium oxide, silica and clay-based ceramics [29–35]. In this study, high-porosity magnetic ceramic bodies to be used as magnetic filters were produced by zinc ferrite nanoparticles using the freeze casting technique.

2. Experimental procedure

2.1. Solution combustion synthesis

Zinc ferrite nanoparticles were obtained from the solution combustion method – a pyrolysis process – using zinc nitrate hexahydrate (Aldrich brand, 98.0% purity), iron nitrate trihydrate (Aldrich brand, 98.0% purity) as ceramic precursors and glycine ($C_2H_5NO_2$) (Aldrich brand, 98.5% purity) as organic fuel. The chosen glycine–nitrate (G/N) ratio was 1.0. The slurry was prepared based on stoichiometric calculation to obtain $ZnFe_2O_4$. After mixing the reagents, an homogeneous solution was obtained and heated up to 100 °C to allow distilled water evaporation, with formation of a highly viscous gel. At this point, the combustion reaction occurred, resulting in the nanostructured powder. The high heating rates involved in the process result in quick exposure of the powder to high synthesis temperatures nucleate small crystallites, as the growth step is almost suppressed. A good advantage is the absence of subsequent heat treatment [21].

2.2. Preparation of the colloidal slurry

The obtained ferrite nanoparticles were dispersed in distilled water, at room temperature and the pH value was adjusted to 10.0 [14] in order to reach the aqueous slurry stability. The solid rate in the slurry was fixed at 10.0% in weight, and the water-soluble polymeric binder PEG-8000 (Aldrich brand) was added to the slurry in 2.0% and 3.0% by weight, relative to the ceramic weight.

2.3. Suspension freezing and drying of samples

The suspension was poured into a polyvinyl chloride (PVC) container with 20.0 mm in diameter and 30.0 mm in length. The PVC container was placed on a copper disk with 50.0 mm in diameter and 5.0 mm thickness, with the top exposed to atmospheric conditions. This set was placed in contact with a cold copper finger. Freezing was performed in liquid nitrogen, with a cooling rate of 10 °C/min, between 10 °C and −145 °C. After reaching the temperature of −145 °C, the samples were kept 0.5 h at this temperature before being retrieved and transfered to a freezer until they were sent to the freeze-drying process by use of a freeze drier. Lyophilization is the step that completes freeze casting, sublimating solid-state water. The used freeze drier was a Labconco model Freezone 2.5, in the following conditions:

- 0.035 mBar of pressure in the chamber;
- 30 h of time for drying.

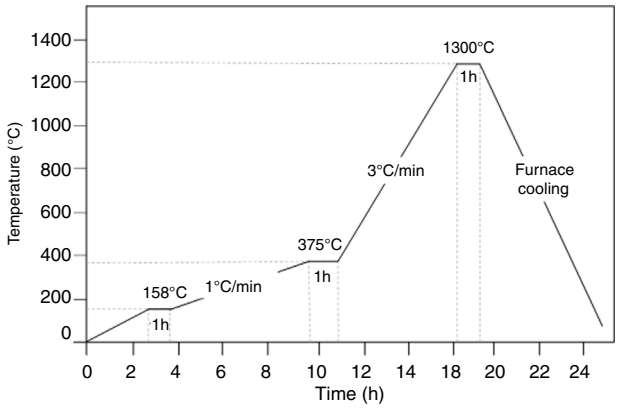

Fig. 1 – Heat treatment steps for polymer binder removal and sintering of samples.

2.4. Sintering

The green bodies were sintered to improve strength and integrity, achieving suitable mechanical resistance. To do so, samples were placed in a platinum crucible and sintering route was designed to carefully eliminate the binder (PEG-8000) without damaging the green body structure, and achieve proper densification of pore walls, according to Fig. 1:

- heating rate of 1 °C/min to 158 °C;
- dwell time of 1 h at 158 °C;
- heating rate of 1 °C/min to 375 °C;
- dwell time of 1 h at 375 °C;
- heating rate of 3 °C/min to 1300 °C;
- dwell time of 1 h at 1300 °C.

2.5. Characterization

Sintered samples were characterized by X-ray diffraction (XRD) in an X'PERT PRO PANalytical diffractometer, with monochromatic radiation (Cu Kα, λ = 1.5406 Å), step size of 0.05° s^{-1}, time per step 150 s and 2θ between 10° and 90°. The pores structure morphology was assessed by a scanning electron microscope (SEM) (FEI model Quanta 250) with field emission gun (FEG), under high vacuum. The nanometric powder density was measured by a pycnometer (AccuPyc II) using helium gas, with measurements performed at room

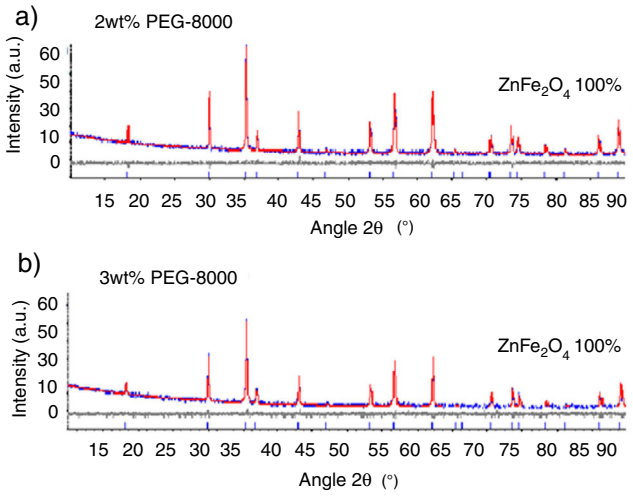

Fig. 2 – XRD patterns of $ZnFe_2O_4$ samples with 2.0wt% PEG-8000 (a) and 3.0wt% PEG-8000 (b).

temperature. Total porosity measurements were assessed by NBR ISO 5017 standard.

3. Results and discussion

3.1. *X-ray diffraction (XRD)*

Fig. 2(a) and (b) shows XRD patterns of samples with 2.0 wt% and 3.0 wt% of PEG-8000, respectively. The XRD patterns were refined using Rietveld's method, by the use of TOPAS-Academic version 4.1. For phases analysis the index card ICSD-91827 was used. Both samples showed ferrite phase as the only present phase, with goodness of fitness (GOF) adjustment of 1.24 and 1.21, as shown in Table 1. There was no phase transformation during sintering and the polymer binder was successfully eliminated. Table 1 shows the parameters obtained by the diffractograms adjustment.

By refining the parameters of sintered samples, it was possible to verify that the sintering process was effective, with crystallite growth and consequent grain growth, starting from nanometric powder.

3.2. *Scanning electron microscopy (SEM)*

The synthesized bodies were observed in cross-section regions of samples, along a direction parallel to freezing front. In Fig. 3(a–f), red arrows represent the freezing direction front of ice crystals.

By SEM analyses, it was possible to confirm the formation of porous channels in freeze direction for both 2.0 wt% and 3.0 wt% binder samples, although it is more evident for 3.0 wt% samples. The formation of lamellar structure, characteristic of ice crystals growth, is also evident, with a columnar freezing front [27,36], essential for application in filtration [37]. The presence of homogeneous spherical pores and cross-linked pores [38], with primary alignments of freezing front and, secondary alignments between the porous channels, derived from the presence of the high molecular weight PEG [39], are shown in Fig. 3(b).

Table 1 – Parameters obtained by the Rietveld's method.

	2.0 wt%	3.0 wt%
GOF	1.24	1.21
Formed phase	$ZnFe_2O_4$	$ZnFe_2O_4$
Crystal structure	Cubic	Cubic
Density [g/cm^3]	5.32	5.32
Crystalitte size [nm]	420.1	229.4
Lattice parameter [Å]	8.44	8.44

Table 2 – Measured values of density, porosity, densification and sintering shrinkage of samples.

	2.0 wt%	3.0 wt%
Apparent density [g/cm^3]	2.83	1.93
Solid apparent density [g/cm^3]	5.48	5.35
Apparent porosity [%]	48.34	63.83
Abosrtion of water [%]	17.10	33.05
Densification [%]	56.24	38.44
Sintering shrinkage [%]	73.64	56.89

3.3. *Measures of density, porosity, densification and sintering shrinkage*

Density of nanometric powders, measured by a pycnometer at room temperature, was 6.6415 g/cm^3 with a standard deviation of 0.0164 g/cm^3. Apparent density of sintered specimens was assessed by the Archimedes' method, following the NBR ISO 5017 standard [40], and the values obtained are presented in Table 2, as well as the values for apparent porosity. These results suggest small fraction of interconnected pores [41], with water absorption of 17.1% and 33.0% for 2.0 wt% and 3.0 wt% of PEG-8000, respectively, whereas the apparent porosity found is below the expected values for 10.0 wt% of solid, when it is compared to other ceramics studies [27]. No cracks were observed in sintered samples, but there was a volumetric shrinkage of 73.0% in the 2.0 wt% PEG-8000 sample and 56.0% in the 3.0 wt% PEG-8000 during sintering. The measurement of volumetric retraction was made by comparing samples diameter and height before and after sintering.

Both high sintering shrinkage and low porosity can be explained by the sintering temperature and route: high temperatures tend to increase densification because sintering is a thermally activated process, which lead to a decrease in porosity, closing pores, changing the structure formed during freezing, and the crystallite growth, as observed by XRD. Low radii ions, such as zinc, with an atomic radius of 0.74 Å, while iron's is 0.77 Å, are easy to diffuse, increasing densification.

It is also evident the role of additive in the slurry stability, growth of ice crystals tips [37], mechanical strength of green bodies before sintering [39] and formation of porous morphology. PEG-8000 increased the viscosity of suspension by reducing porosity, with linear and volumetric shrinkage of ceramic bodies. This effect is similar to that observed in processes using gelatin as solvent [38,39]. The increase from 2.0 wt% to 3.0 wt% of PEG provided higher porosity in the

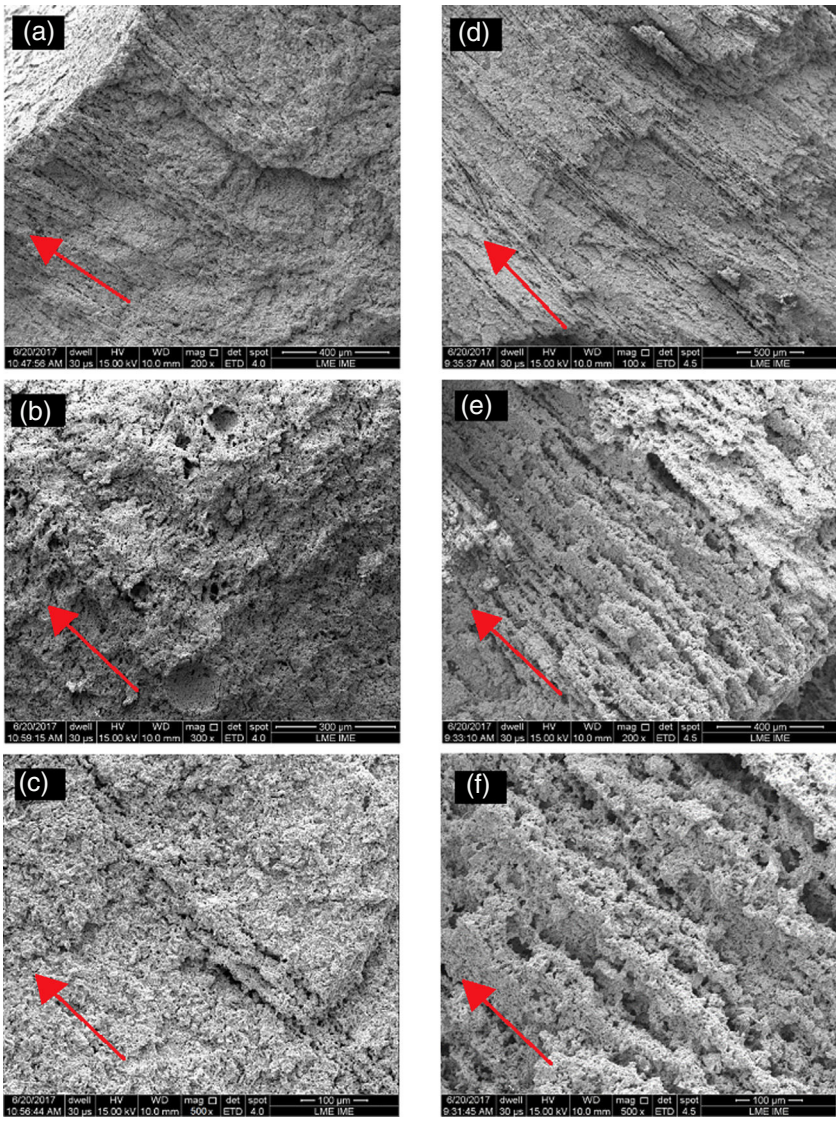

Fig. 3 – SEM micrographs of $ZnFe_2O_4$ sintered with 2.0wt% PEG-8000 (a–c), and with 3.0wt% of PEG-8000 (d–f).

ceramic bodies, delaying the process of grains coalescence, because the high molecular weight PEG tends to form thin porous channels [37].

4. Conclusions

Two magnetic filters were produced, made of zinc ferrite nanoparticles, by the freeze casting technique, with 2.0 wt% and 3.0 wt% of PEG – 8000 as binder. The sintered bodies showed porosities of 48.0% and 63.0%, respectively. Due to the high molecular weight of PEG used, the studied samples did not show expected porosity values for percentage of solids added. However, low molecular weight PEG is being considered in future woks in order to obtain higher porosity values.

Conflicts of interest

The authors declare no conflicts of interest.

Acknowledgments

The authors are grateful to the Mechanical and Materials Engineering Department of the Military Engineering Institute, X-ray Crystallography and Diffraction Laboratory of the Brazilian Center for Physical Research and the Center for Mineral Technology for their assistance in conducting the tests and analyzes and CNPq by financial support under grant number 141012/2017-0.

REFERENCES

[1] Ibrahim A, Couvreur P, Roland M, Speiser P. New magnetic drug carrier. J Pharm Pharmacol 1983;35(1):59–61, http://dx.doi.org/10.1111/j.2042-7158.1983.tb04269.x. Wiley-Blackwell.
[2] Dias MHM, Lauterbur PC. Ferromagnetic particles as contrast agents for magnetic resonance imaging of liver and spleen.

Magn Reson Med 1986;3(2):328–30, http://dx.doi.org/10.1002/mrm.1910030218. Wiley-Blackwell.
[3] Pouliquen D, Perdrisot R, Ermias A, Akoka S, Jallet P, Le Jeune JJ. Superparamagnetic iron oxide nanoparticles as a liver MRI contrast agent: contribution of microencapsulation to improved biodistribution. Magn Reson Imaging 1989;7(6):619–27, http://dx.doi.org/10.1016/0730-725x(89)90530-4. Elsevier BV.
[4] Anton I, de Sabata I, Vékás L. Application orientated researches on magnetic fluids. J Magn Magn Mater 1990;85(1–3):219–26, http://dx.doi.org/10.1016/0304-8853(90)90056-v. Elsevier BV.
[5] Chinnasamy CN, Narayanasamy A, Ponpandian N, Chattopadhyay K, Guérault H, Greneche J-M. Magnetic properties of nanostructured ferrimagnetic zinc ferrite. J Phys: Condens Matter 2000;13(5):7795–805.
[6] Sugimoto M. The past, present, and future of ferrites. J Am Ceram Soc 2004;82(2):269–80, http://dx.doi.org/10.1111/j.1551-2916.1999.tb20058.x. Wiley-Blackwell.
[7] Tsuzuki T. Commercial scale production of inorganic nanoparticles. Int J Nanotechnol 2009;6(5/6):567–78, http://dx.doi.org/10.1504/ijnt.2009.024647. Interscience Publishers.
[8] Iwauchi K. Dielectric properties of fine particles of Fe3O4 and some ferrites. Jpn J Appl Phys 1971;10(11):1520–8, http://dx.doi.org/10.1143/jjap.10.1520. Japan Society of Applied Physics.
[9] Hasmonay E, Depeyrot J, Sousa MH, Tourinho FA, Bacri J-C, Perzynski R, et al. Magnetic and optical properties of ionic ferrofluids based on nickel ferrite nanoparticles. J Appl Phys 2000;88(11):6628–35, http://dx.doi.org/10.1063/1.1288016. AIP Publishing.
[10] Arulmurugan R, Vaidyanathan G, Sendhilnathan S, Jeyadevan B. Mn–Zn ferrite nanoparticles for ferrofluid preparation: study on thermal–magnetic properties. J Magn Magn Mater 2006;298(2):83–94, http://dx.doi.org/10.1016/j.jmmm.2005.03.002. Elsevier BV.
[11] Guskos N, Glenis S, Typek J, Zolnierkiewicz G, Berczynski P, Walrdal K, et al. Magnetic properties of $ZnFe_2O_4$ nanoparticles. Open Phys 2012;10(2):470–7, http://dx.doi.org/10.2478/s11534-012-0013-3. Walter de Gruyter GmbH.
[12] Shahraki RR, Ebrahimi M, Ebrahimi SAS, Masoudpanah SM. Structural characterization and magnetic properties of superparamagnetic zinc ferrite nanoparticles synthesized by the coprecipitation method. J Magn Magn Mater 2012;324(22):3762–5, http://dx.doi.org/10.1016/j.jmmm.2012.06.020. Elsevier BV.
[13] Rameshbabu R, Ramesh R, Kanagesan S, Karthigeyan A, Ponnusamy S. Synthesis and study of structural, morphological and magnetic properties of ZnFe2O4 nanoparticles. J Supercond Novel Magn 2013;27(6):1499–502, http://dx.doi.org/10.1007/s10948-013-2 66-z. Springer Nature.
[14] Shahraki RR, Ebrahim SAS, Masoudpanah SM. Synthesis and characterization of superparamagnetic zinc ferrite–chitosan composite nanoparticles. J Supercond Novel Magn 2015;28(7):2143–7, http://dx.doi.org/10.1007/s10948-015-3015-8. Springer Nature.
[15] Aslibeiki B, Kameli P, Ehsani MH. $MnFe_2O_4$ bulk, nanoparticles and film: a comparative study of structural and magnetic properties. Ceram Int 2016;42(11):12789–95, http://dx.doi.org/10.1016/j.ceramint. 2016.05.041. Elsevier BV.
[16] Seip CT, Carpenter EE, O'Connor CJ, John VT, Li S. Magnetic properties of a series of ferrite nanoparticles synthesized in reverse micelles. IEEE Trans Magn 1998;34(4):1111–3, http://dx.doi.org/10.1109/20.706388. Institute of Electrical and Electronics Engineers (IEEE).
[17] Liu C, Rondinone AJ, Zhang ZJ. Synthesis of magnetic spinel ferrite $CoFe_2O_4$ nanoparticles from ferric salt and characterization of the size-dependent superparamagnetic properties. Pure Appl Chem 2000;72(1–2):37–45, http://dx.doi.org/10.1351/pac200072010037. Walter de Gruyter GmbH.
[18] Nalbandian L, Delimitis A, Zaspalis VT, Deliyanni EA, Bakoyannakis DN, Peleka EN. Hydrothermally prepared nanocrystalline Mn–Zn ferrites: synthesis and characterization. Micropor Mesopor Mater 2008;114(1–3):465–73, http://dx.doi.org/10.1016/j.micromeso.2008.01.034. Elsevier BV.
[19] Naseri MG, Saion EB, Ahangar HA, Hashim M, Shaari AH. Synthesis and characterization of manganese ferrite nanoparticles by thermal treatment method. J Magn Magn Mater 2011;323(13):1745–9, http://dx.doi.org/10.1016/j.jmmm.2011.01.016. Elsevier BV.
[20] Huang M, Quin M, Cao Z, Jia B, Chen P, Wu H, et al. Magnetic iron nanoparticles prepared by solution combustion synthesis and hydrogen reduction. Chem Phys Lett 2016;657:33–8, http://dx.doi.org/10.1016/j.cplett.2016.05.043. Elsevier BV.
[21] Rahaman MN. Ceramic processing. Missouri, USA: CRC Press; 2006. p. 550.
[22] Rudge SR, Kurtz TL, Vessely CR, Catterall LG, Williamson DL. Preparation, characterization, and performance of magnetic iron–carbon composite microparticles for chemotherapy. Biomaterials 2000;21(14):1411–20, http://dx.doi.org/10.1016/s0142-9612(00)00006-5. Elsevier BV.
[23] Cunningham CH, Arai T, Yang PC, Mcconnell MV, Pauly JM, Conolly SM. Positive contrast magnetic resonance imaging of cells labeled with magnetic nanoparticles. Magn Reson Med 2005;53(5):999–1005, http://dx.doi.org/10.1002/mrm.20477. Wiley-Blackwell.
[24] Yi DK, Lee SS, Ying JY. Synthesis and applications of magnetic nanocomposite catalysts. Chem Mater 2006;18(10):2459–61, http://dx.doi.org/10.1021/cm052885p. American Chemical Society (ACS).
[25] Arruebo M, Pacheco RF, Ibarra MR, Santamaría J. Magnetic nanoparticles for drug delivery. Nano Today 2007;2(3):22–32, http://dx.doi.org/10.1016/s1748-0132(07)70084-1. Elsevier BV.
[26] Mahdavian AR, Mirrahimi MA. Efficient separation of heavy metal cations by anchoring polyacrylic acid on superparamagnetic magnetite nanoparticles through surface modification. Chem Eng J 2010;159(1–3):264–71, http://dx.doi.org/10.1016/j.cej.2010.02.041. Elsevier BV.
[27] Deville S. Freeze-casting of porous ceramics: a review of current achievements and issues. Adv Eng Mater 2008;10(3):155–69, http://dx.doi.org/10.1002/adem.2007 00270. Wiley-Blackwell.
[28] Marçal RLSB, Louro LHL. Freeze casting: uma alternativa moderna ao processamento cerâmico. Revista Militar de Ciência e Tecnologia 2016;XXXIII:28–32.
[29] Fukasawa T, Ando M, Ohji T, Kanzaki S. Synthesis of porous ceramics with complex pore structure by freeze-dry processing. J Am Ceram Soc 2001;84(1):230–2, http://dx.doi.org/10.1111/j.1151-2916.2001.tb00638.x. Wiley-Blackwell.
[30] Fukasawa T, Deng Z-Y, Ando M, Ohji T, Goto Y. Pore structure of porous ceramics synthesized from water-based slurry by freeze-dry process. J Mater Sci 2001;36(10):2523–7, http://dx.doi.org/10.1023/a:1017946518955. Springer Nature.
[31] Fukasawa T, Deng Z-Y, Ando M, Ohji T, Kanzaki S. Synthesis of porous silicon nitride with unidirectionally aligned channels using freeze-drying process. J Am Ceram Soc 2002;85(9):2151–5,

http://dx.doi.org/10.1111/j.1151-2916.2002.tb00426.x. Wiley-Blackwell.

[32] Tang J, Chen YF, Wang H, Liu HL, Fan QS. Preparation of oriented porous silicon carbide bodies by freeze-casting process. Key Eng Mater 2005;280–283:1287–90, http://dx.doi.org/10.4028/www.scientific.net/kem.280-283.1287. Trans Tech Publications.

[33] Sepúlveda R, Plunk AA, Dunand DC. Microstructure of Fe_2O_3 scaffolds created by freeze-casting and sintering. Mater Lett 2015;142:56–9, http://dx.doi.org/10.1016/j.matlet.2014.11.155. Elsevier BV.

[34] Park H, Choi M, Choe H, Dunand DC. Microstructure and compressive behavior of ice-templated copper foams with directional, lamellar pores. Mater Sci Eng A 2017;679:435–45, http://dx.doi.org/10.1016/j.msea.2016.10.057. Elsevier BV.

[35] Plunk AA, Dunand DC. Iron foams created by directional freeze casting of iron oxide, reduction and sintering. Mater Lett 2017;191:112–5, http://dx.doi.org/10.1016/j.matlet.2016.12.104. Elsevier BV.

[36] Deville S, Saiz E, Tomsia AP. Ice-templated porous alumina structures. Acta Mater 2007;55(6):1965–74, http://dx.doi.org/10.1016/j.actamat.2006.11.003. Elsevier BV.

[37] Liu R, Xu T, Wang C. A review of fabrication strategies and applications of porous ceramics prepared by freeze-casting method. Ceram Int 2016;42(2):2907–25, http://dx.doi.org/10.1016/j.ceramint.2015.10.148. Elsevier BV.

[38] Zhang Y, Zuo K, Zeng Y-P. Effects of gelatin addition on the microstructure of freeze-cast porous hydroxyapatite ceramics. Ceram Int 2009;35(6):2151–4, http://dx.doi.org/10.1016/j.ceramint.2008.11.022. Elsevier BV.

[39] Pekor C, Nettleship I. The effect of the molecular weight of polyethylene glycol on the microstructure of freeze-cast alumina. Ceram Int 2014;40(7):9171–7, http://dx.doi.org/10.1016/j.ceramint.2014.01.134. Elsevier BV.

[40] Associação Brasileira de Normas Técnicas. NBR ISO 5017:2015: Produtos refratários conformados densos – Determinação da densidade de massa, porosidade aparente e porosidade real. Rio de Janeiro; 2015. p. 7.

[41] Silva AMA, Nunes EHM, Souza DF, Martens DL, Da Costa JCD, Houmard M, Vasconcelos WL. The influence of Fe_2O_3 doping on the pore structure and mechanical strength of TiO_2-containing alumina obtained by freeze-casting. Ceram Int 2015;41(10):14049–56, http://dx.doi.org/10.1016/j.ceramint.2015.07.021. Elsevier BV.